



**HAL**  
open science

## Vortical flow structures induced by red blood cells in capillaries

François Yaya, Johannes Römer, Achim Guckenberg, Thomas John, Stephan Gekle, Thomas Podgorski, Christian Wagner

► **To cite this version:**

François Yaya, Johannes Römer, Achim Guckenberg, Thomas John, Stephan Gekle, et al.. Vortical flow structures induced by red blood cells in capillaries. *Microcirculation*, 2021, 28 (5), 10.1111/micc.12693 . hal-03358459

**HAL Id: hal-03358459**

**<https://hal.science/hal-03358459>**

Submitted on 29 Sep 2021

**HAL** is a multi-disciplinary open access archive for the deposit and dissemination of scientific research documents, whether they are published or not. The documents may come from teaching and research institutions in France or abroad, or from public or private research centers.

L'archive ouverte pluridisciplinaire **HAL**, est destinée au dépôt et à la diffusion de documents scientifiques de niveau recherche, publiés ou non, émanant des établissements d'enseignement et de recherche français ou étrangers, des laboratoires publics ou privés.

# Vortical flow structures induced by red blood cells in capillaries

François Yaya<sup>1,2</sup> | Johannes Römer<sup>3</sup> | Achim Guckenberger<sup>3</sup> | Thomas John<sup>1</sup> |  
Stephan Gekle<sup>3</sup>  | Thomas Podgorski<sup>2</sup>  | Christian Wagner<sup>4,5</sup> 

<sup>1</sup>Experimental Physics, Saarland University, Saarbrücken, Germany

<sup>2</sup>Laboratoire Interdisciplinaire de Physique, Saint Martin d'Hères, France

<sup>3</sup>Biofluid Simulation and Modeling, Theoretische Physik VI, Universität Bayreuth, Bayreuth, Germany

<sup>4</sup>Experimental Physics, Saarland University, Saarbrücken, Germany

<sup>5</sup>Physics and Materials Science Research Unit, University of Luxembourg, Luxembourg City, Luxembourg

## Correspondence

Christian Wagner, Experimental Physics, Saarland University, Campus Building E2 6, Saarbrücken, Germany.  
Email: c.wagner@mx.uni-saarland.de

## Funding information

Deutsche Forschungsgemeinschaft; Centre National d'Etudes Spatiales; Labex; French German University

## Abstract

**Objective:** Knowledge about the flow field of the plasma around the red blood cells in capillary flow is important for a physical understanding of blood flow and the transport of micro- and nanoparticles and molecules in the flowing plasma. We conducted an experimental study on the flow field around red blood cells in capillary flow that is complemented by simulations of vortical flow between red blood cells.

**Methods:** Red blood cells were injected in a  $10 \times 12 \mu\text{m}$  rectangular microchannel at a low hematocrit, and the flow field around one or two cells was captured by a high-speed camera that tracked 250 nm nanoparticles in the flow field, acting as tracers.

**Results:** While the flow field around a steady "croissant" shape is found to be similar to that of a rigid sphere, the flow field around a "slipper" shape exhibits a small vortex at the rear of the red blood cell. Even more pronounced are vortex-like structures observed in the central region between two neighboring croissants.

**Conclusions:** The rotation frequency of the vortices is to a good approximation, inversely proportional to the distance between the cells. Our experimental data are complemented by numerical simulations.

## KEYWORDS

flow, particle tracking velocimetry, simulations

## 1 | INTRODUCTION

Besides its physiological relevance, blood flow in microcapillaries is a prime example of a biological fluid-structure interaction problem between the elastic red blood cells (RBCs) and the hydrodynamic flow of plasma.<sup>1–3</sup> Over recent years, quite some attention has been paid to the dynamics of RBCs in cylindrical or rectangular channels, which are known to be the most common configurations in model microfluidic flows. Depending on external parameters such as flow speed, channel size, and plasma viscosity, two main shapes have emerged from these experimental<sup>4–9</sup> as

well as numerical studies.<sup>9–18</sup> The first, called "slipper", is an elongated, non-axisymmetric shape in which the RBCs tend to flow at a steady position slightly away from the channel center. The second one, almost axis-symmetric in cylindrical capillaries and with two planes of symmetry in rectangular channels, is termed "parachute" in cylindrical tubes or "croissant" in rectangular cross-sections and flows in the channel center. In addition, some works reported on observations of clusters of two or more RBCs formed without any molecular interactions that can be induced by the plasma molecules (often referred to as rouleaux formation) but kept together with a certain distance of a few microns in-between the cells by

**Abbreviations:** BI, boundary integral; BSA, bovine serum albumin; PBS, phosphate buffer saline; PDMS, polydimethylsiloxane; PTV, particle tracking velocimetry; RBCs, red blood cells.

This is an open access article under the terms of the Creative Commons Attribution License, which permits use, distribution and reproduction in any medium, provided the original work is properly cited.

© 2021 The Authors. *Microcirculation* published by John Wiley & Sons Ltd.

hydrodynamic interactions.<sup>19–26</sup> While there is good agreement between numerical simulations and experiments regarding the actual shape of RBCs, less attention has been paid to resolve the flow field of the surrounding plasma experimentally. While in the absence of RBCs, the flow would be a simple parabolic Poiseuille profile, the presence of RBCs strongly disturbs the flow.<sup>27</sup> Understanding the actual flow pattern is essential, for example, for the distribution of nanometric drug delivery agents or dissolved substances in microcapillary blood flow<sup>26,28–35</sup> as well as to understand the nature of interactions between cells. For a simple sphere in a cylindrical channel, the flow pattern can be computed analytically, but nevertheless results in surprisingly intricate dynamics of the solute.<sup>36</sup> While there is quite some literature on the flow field in microchannels around rigid or only slightly deformable objects such as microspheres or droplets,<sup>37–40</sup> experimental data are rare for the complex flows arising due to the above-described croissant and slipper motions of red blood cells. In RBC clusters, computer simulations have indicated the presence of vortex-like structures between neighboring RBCs.<sup>19,20,22,26</sup> Here, we present experimental observations of (i) the flow around isolated RBCs and (ii) the vortical flow between clustering RBCs in a rectangular microchannel using particle tracking. We find that the rotation frequency of the vortices scales inversely proportional to the RBC distance. Our particle tracking measurements are in reasonable agreement with corresponding boundary-integral (BI) simulations.

## 2 | MATERIAL AND METHODS

### 2.1 | Experiments

To mimic blood capillaries, we used rectangular straight channels of 12  $\mu\text{m}$  width, 10  $\mu\text{m}$  depth, and about 40 mm in length as microfluidic chips. The camera was positioned such that the long (12  $\mu\text{m}$ ) side was viewed in the images. Channels were made from polydimethylsiloxane (PDMS).<sup>41</sup> To avoid RBCs adhering onto the walls, the channels were flushed with a buffer solution containing BSA at 1%. The flow of the suspension was observed in a microscope with an oil-immersion objective (Nikon CFI Plan Fluor 60x, NA 1.25). The field of observation was at 10 mm away from the pressure inlet above the microfluidic chip. We used a high-speed camera (HiSpec Fastec 2G) to record image sequences at frame rates of 9000 fps. We investigated the flow at cell speeds at a physiologically relevant parameter range and beyond, from 1 mm/s up to 10 mm/s. The various flow and cell speeds were achieved with a pressure controller (Elveflow OB1+) at pressure drops ranging from 100 to 1000 mbar, respectively.<sup>9</sup>

To visualize the flow field around the moving RBC, we added nanoparticles with a surface coating of polyethylene glycol (PEG) and measuring 250 nm in diameter (MicroMod) in an aqueous solution containing 0.1% of BSA. Blood was drawn from healthy donors after giving an informed consent in compliance with the ethical requirements of Saarland University, Saarbrücken, Germany

(Ärztekammer des Saarlandes, approval number 24/12). We used a suspension of washed RBCs in phosphate-buffered saline (PBS) at 0.5% hematocrit with nanoparticles as tracers. Samples were mixed regularly to prevent the sedimentation of RBCs. The shape and speed of individual cells depended on the applied pressure drop and remained stationary within the time of observation in our experiments. We observed two main steady cell shapes in our rectangular channel geometries: croissants at rather low flow speeds and slippers at higher flow speeds, Figure 1. We determined the speed of the RBCs from the recorded image sequence over a distance of 100  $\mu\text{m}$ . The trajectories of the tracers were determined using our own MATLAB code in the co-moving frame of the individual RBC.

Figure 1A and B (Multimedia view) shows typical trajectories of tracers as overlaid images of snapshots of a flowing RBCs for two different velocities. The motion of tracers between two RBCs is studied in a similar manner. During the observation time span, the distance  $d_{\text{RBC}}$  between two consecutive RBCs never changed more than 10% in our experiments; that is, both cells had comparable velocities.

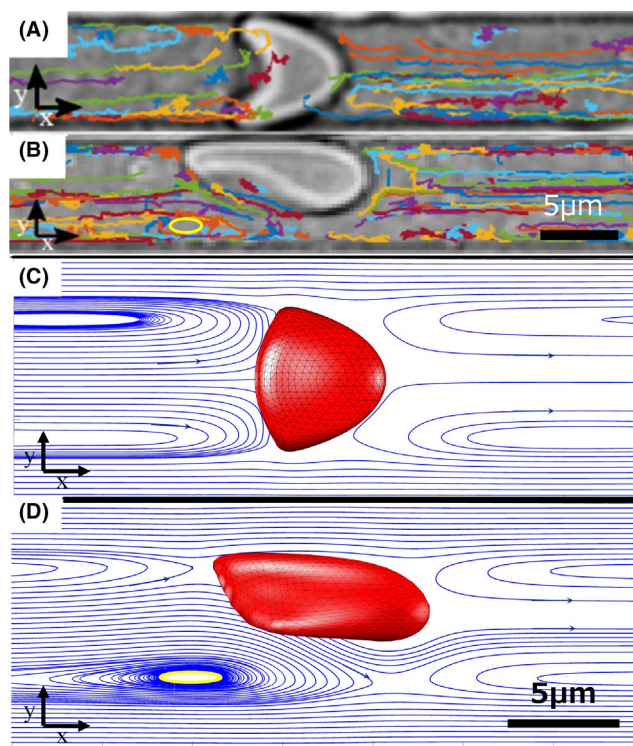


**FIGURE 1** Snapshots of RBCs in (A) croissant and (B) slipper shape, together with an overlay of experimental recorded trajectories of tracers. Images (C) and (D) represent the streamlines and cell shapes from the numerical simulations in the central plane of the channel. The speed in (A) and (C) is  $v_{\text{RBC}} = 2.83 \text{ mm s}^{-1}$  and in (B) and (D)  $v_{\text{RBC}} = 6.50 \text{ mm s}^{-1}$ . A closed vortex can be seen (in yellow) in both (B) and (D). Particle trajectories and streamlines are shown in the co-moving frame of the RBCs. The fluid flows from left to right, and RBCs appear to be closer to the walls in (A) and (B) due to the camera's position. Experimental videos from (A) and (B) can be found in Supplementary Material (Multimedia view)

## 2.2 | 3D simulations

In brief, our 3D boundary-integral simulations solved the Stokes equations for the fluid inside and outside the red blood cell,<sup>9,42,43</sup> which is justified by the small Reynolds number of approximately 0.1. A specific advantage of BI simulations is that the full instantaneous flow field at any time can be computed knowing only the parabolic background flow, the forces on the channel wall, and the RBC membrane.<sup>42,43</sup> Time integration is not necessary to compute the flow field. In our model, the membrane forces were computed following the models by Skalak and Helfrich for shear, area, and bending elasticity, respectively.<sup>2,44,45</sup> At the membrane, we applied a no-slip boundary condition as well as a stress jump between the interior and exterior fluid which is caused by membrane elasticity. Periodic boundary conditions along the channel were used with a computation window length of 42  $\mu\text{m}$ . This length was sufficient to recover a nearly undisturbed Poiseuille flow far away from the cell. For the velocity field computation, a snapshot of the simulation was selected and the shape of the RBC at that time was frozen. Then, the velocity field was computed on a regular grid in the central plane and transformed to the frame of reference of the moving RBC using its center-of-mass velocity. As the slipper exhibited periodic oscillations through a series of slightly varying shapes, an arbitrary shape out of these was selected for computing the streamlines, following the procedure described above. In an ideal situation, the mirror symmetry of the system around the central plane would forbid the existence of out-of-plane currents. Due to rounding and discretization errors, small spurious out-of-plane currents may nevertheless arise, which however were set to zero.

The simulations were performed in the same channel geometry as the experiments. Figure 1C and D shows the converged 3D RBC shapes and corresponding streamlines in the channel middle plane for a croissant and a slipper, respectively. To compute the streamlines between two cells in a cluster, we selected a converged croissant shape from the simulation with a single RBC at the corresponding speed. This shape was then copied, and both cells placed into the channel. At steady state, the distance  $d_{\text{RBC}}$  between two RBCs in a cluster is constant and depends on the flow velocity. However, in the experiments many distortions can disturb the equilibrium distance positions and different distances can be observed for the same flow condition. This also means that the clusters are not yet at their converged distance. To mimic this situation in the simulations, we placed two cells with the approximated shape at the desired distance in the channel. After a short time span of typically 70 ms, the streamlines were computed starting at a vertical line between the two cells. The reference frame is the center-of-mass velocity of the left RBC. Streamlines contain only directional information but no absolute velocities which are needed to compute the rotation period of particles trapped in flow vortices. To obtain this information, we place virtual tracer particles (again starting from a line of seed points) and integrate their trajectory in time given the flow field extracted from BI

simulations (which is assumed to be stationary). This procedure allowed us to obtain not only the particle trajectories, but also the temporal information such as rotation periods. In addition, Figure 5 shows particle trajectories integrated backward in time in order to demonstrate the possibility of particle escape from the central vortices in non-perfectly symmetric situations.

## 3 | RESULTS

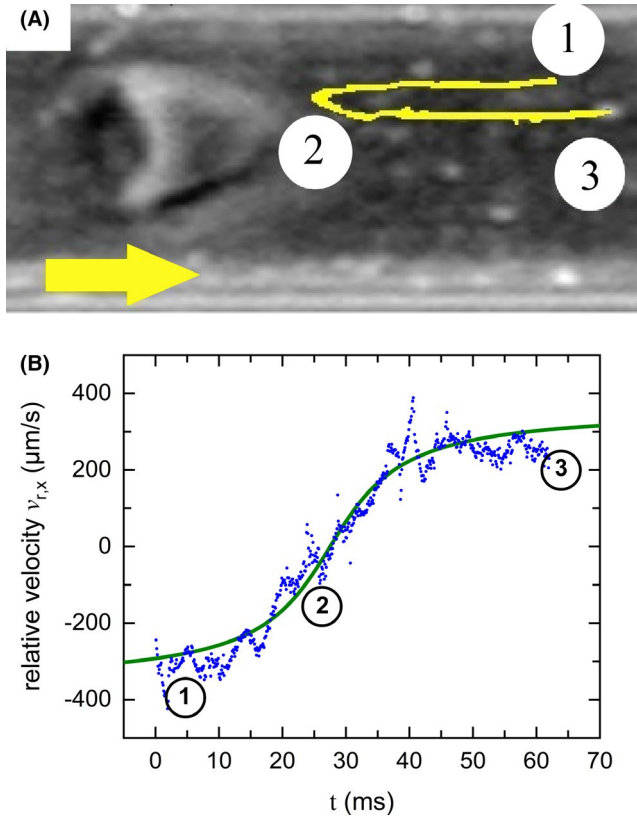
### 3.1 | Flow field in the vicinity of a single RBC

Figure 1 shows the experimental and numerical results of our flow field measurements around the two characteristic cell shapes. Far away from the cell, the velocity profile in the rectangular channel is almost parabolic.<sup>46</sup> The speed of the RBCs is approximately the mean velocity of the free liquid flow in the channel because the volume flux is conserved. The cell speed defines the speed of the co-moving frame and is always lower than the fluid velocity in the middle of the channel far away from the cell.

At low flow speeds, the observed cell shape is a symmetric croissant Figure 1A and C.<sup>9</sup> As depicted by the blue arrows following the streamlines (Figure 1C), tracers in the middle of the channel and in front of the cell move away from the cell. Tracers move toward the cell when they are situated in the middle, behind the cell. In the co-moving frame, the flow velocity is zero at the cell surface and there is a stagnation point on the cell surface on the center line. Closer to the walls, this flow direction is reversed. The combination of those motions leads to a strongly elongated half ellipse for the trajectory of a single tracer. These streamlines are comparable to what was observed experimentally for flowing droplets in microchannels.<sup>39</sup>

From the experimental particle tracking velocimetry (PTV) of the tracers, we can also deduce the relative velocity in the co-moving frame  $\vec{v}_r$ . The component in flow direction  $v_{r,x}$  is shown as function of time in Figure 2B.

The velocity can be fitted with a heuristic sigmoidal function. Obviously, tracers decelerate when approaching the cell and accelerate to the faster fluid motion in the middle of the channel when they move away from the cell. With our microscopic setup, we imaged the full sample height, and therefore, the observed position of tracers was always their projection in the  $x$ - $y$  plane. Therefore, we also observed trajectories that approach and depart from the cell in the  $y = 0$  plane (Figure 1A). This is especially the case when the tracer's motion is in the orthogonal plane with respect to the plane of projection. At higher flow speeds, the cells attain a slipper shape.<sup>9</sup> In this asymmetric configuration, a vortical flow can be observed behind the cell (see Figure 1B) even though the flow remains laminar. The slipper shape and the existence of the vortices are confirmed by our numerical simulations (Figure 1D). However, a fully closed vortex flow in the middle plane of the channel as predicted from the numerical simulations could not be seen in the experimental situation where



**FIGURE 2** Motion of tracers in the co-moving frame of a RBC in croissant shape flowing with a speed of  $v_{\text{RBC}} = (4.3 \pm 0.1) \text{ mm s}^{-1}$ . A, Snapshot of the RBC with an overlay of a tracer trajectory from the image sequence. B, The velocity  $v_{r,x}$  in the flow direction of the tracer when it approaches and recedes from the cell. The fit curve is an empirical sigmoid function. The flow direction of the cell is indicated by a yellow arrow in, and the path of motion is indicated by numbers: (1) The tracer approaches the RBC, and (2) its relative speed in the co-moving frame of the RBC is negligible and (3) finally moves away from the RBC with an absolute speed comparable to its arrival

small irregularities are enough to displace tracer particles out of the vortex zone. This indicates that in realistic situations it will be unlikely that particles will be trapped in such a vortex. In both cases, for croissants as well as for slippers, the presence of RBCs reduces the spatial variations in fluid velocities over the channel width to an almost plug-like flow, and therefore, the spreading of suspended tracers in the flow direction over the channel is also reduced. This becomes even more pronounced for clusters of two RBCs as we will see in the following.

### 3.2 | Flow field in the vicinity of a cluster of two RBCs

At low hematocrit levels, the mean distance between consecutive RBCs in the channel is typically very large compared with the cell's size and the channel width. If two cells come close to each other, however, they can form a stable cluster due to their

hydrodynamic interaction.<sup>19–26</sup> A significant amount of the liquid between the cells seems to be “encapsulated” and does not mix anymore with the liquid outside of the cluster. Similarly, to the tracer trajectories of single cells, we observed hairpin loops and vortices for tracers moving in the plane of observation and straight lines for tracers moving orthogonal to it (Figure 3A (Multimedia view)), as a consequence of our optical projection. Our numerical simulations confirm that the streamlines correspond to a toroidal vortex, just similar to smoke rings, with the axis of symmetry along the channel in the  $+x$ -direction, Figure 3B. In the co-moving frame, the channel borders move with the speed of the RBC-cluster in the  $-x$ -direction. This relative border motion drives the rotation of the liquid between the cells, similar to the case of a lid-driven cavity flow,<sup>47</sup> and those types of vortices have been observed in the case of flowing droplets in microfluidic devices.<sup>40</sup> Accordingly, the liquid in the inner part of the channel moves in the  $+x$ -direction with a speed that is somewhat higher than the speed of the cells in the laboratory frame.

Here, we analyze only the flow field of clusters of two croissant-shaped cells. To characterize the torus movement of the tracers more quantitatively, we consider the period  $T$  for one cycle. The vortex forms a deformed torus in 3D and that the flow becomes faster with increasing distance from the central axis of revolution. Figure 4 shows the period  $T$  as a function of the distance between the two cells,  $d_{\text{RBC}}$ . The period increases almost linearly with the distance, both for the simulated and for the experimental results. As a first approximation, a tracer is considered to move along the circumference  $C$  of an ellipse. The period  $T$  was experimentally determined by measuring the elapsed time needed by a tracer to complete a revolution between two croissants separated by the distance  $d_{\text{RBC}}$ . In simulations, since more periods can be obtained, the period  $T$  corresponds to an arithmetic average of the collected periods. As can be seen in Figure 2B, the relative velocity of a tracer is not constant. However, to obtain an analytical expression for the period  $T$  we assume a constant tracer speed  $v_t$  along a particular ellipse circumference drawn by the tracer and  $v_t$  is chosen to be the fitting parameter. The period  $T(d_{\text{RBC}})$  is given by the ratio of  $C$  and  $v_t$ . Within concentric ellipses and with decreasing sizes, the velocity  $v_t$  decreases as well. The extension of the largest ellipse is given by an almost constant semi-minor axis  $a$  in order of a quarter of the channel width and a major axis  $d_{\text{RBC}}$  in the order of the interior distance between two cells. Using a truncated series expansion for the circumference  $C$  of the largest ellipse (details in the Supporting Information), the estimated period  $T(d_{\text{RBC}})$  is given by:

$$T(d_{\text{RBC}}) = \frac{C}{v_t} = \frac{\pi}{v_t} \left( a + \frac{d_{\text{RBC}}}{2} \right) \left( 1 + \frac{\theta^2}{4} \right) \quad (1)$$

with:  $\theta = (a - d_{\text{RBC}}/2) / (a + d_{\text{RBC}}/2)$

This relationship appears valid for both experiments and simulations. In fact, both show that tracer velocities  $v_t$  in the co-moving frame happen to be lower than the velocity of a cell  $v_{\text{RBC}}$  in the

**FIGURE 3** A, Snapshot of a cluster of two RBCs in croissant shape with a distance of  $d_{\text{RBC}} = 5.2 \mu\text{m}$  together with an overlay of tracer trajectories. The liquid between the cells seems to be encapsulated in a vortex and to rotate as a torus with the axis of symmetry in  $x$ -direction. B, Numerical simulation of a cluster. The streamlines indicate how tracers will be transported from the middle along helical trajectories (Figure 6). An experimental video from (A) can be found in Supplementary Material (Multimedia view)

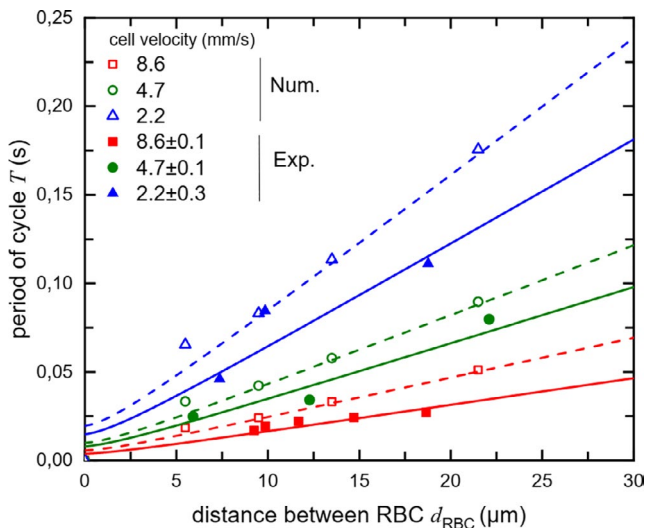
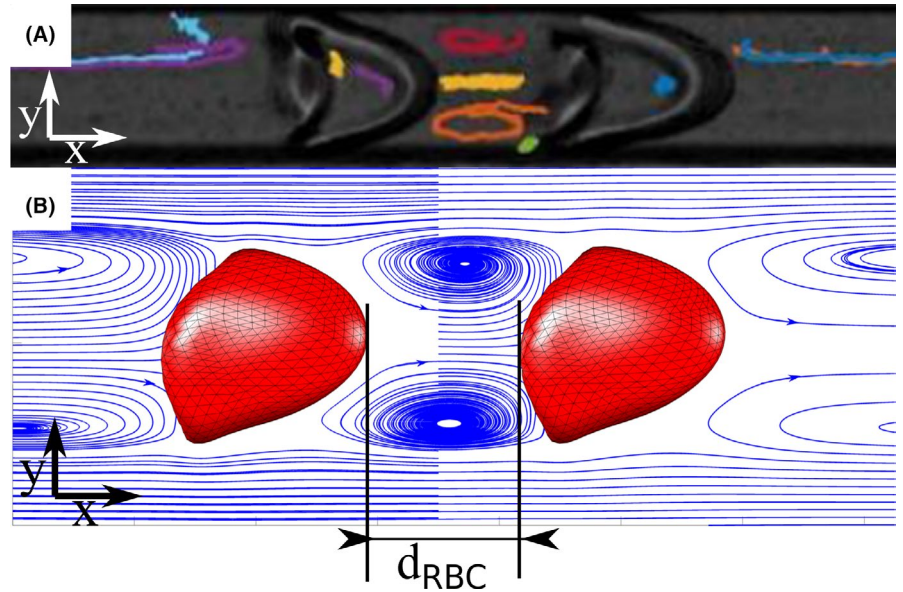


**FIGURE 4** Period of cycles for a toroidal tracer motion between two RBCs as a function of the distance between the cells. Experimental data are represented by solid symbols and lines and numerical results by open symbols and dashed lines, respectively. The fit represents a motion on an axial stretched torus with ellipses of revolution. It is based on Equation (1), with  $\pi/v_t$  as a fitting parameter and the minor axis fixed as  $a = 3 \mu\text{m}$  (Supplementary Material)

laboratory frame. However, there are some quantitative differences between the simulated and experimental periods which we attribute to the fact that the cells at various distances are not in their equilibrium situation. This is even more pronounced for larger distances  $d_{\text{RBC}}$  between the RBCs. We show in Figure 4 the extracted periods as a function of the distance between two RBCs flowing at different speeds. As expected, an offset on the period ( $y$ -axis) can be observed due to the fact that the semi-minor axis  $a$  is considered constant. We found in simulations that proper vortices were rarely formed for  $d_{\text{RBC}} > 40 \mu\text{m}$ . In this case, a tracer

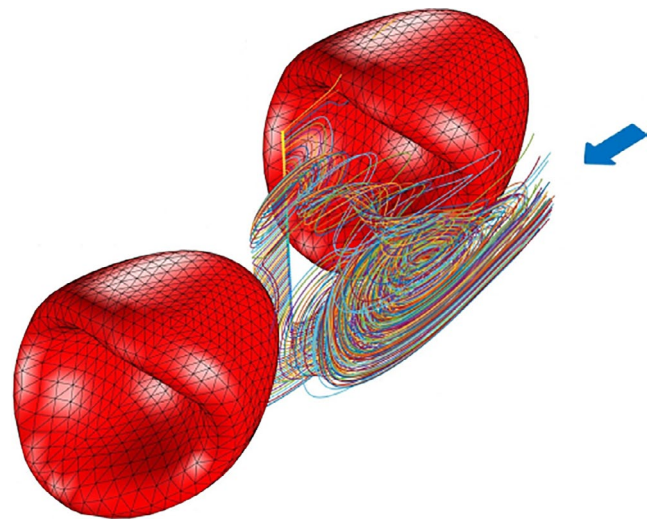


**FIGURE 5** 3D view showing the provenance (blue arrow) of the tracers and their trajectories for a cell velocity of  $2.2 \text{ mm s}^{-1}$

escapes the vortex before doing a full revolution. For distances shorter than  $5 \mu\text{m}$ , no vortex could be observed in the experiments. This is in agreement with simulations<sup>19</sup> that define the “vortex existence” boundary to be  $1.4 R_0$  with  $R_0$  being the effective radius of a RBC.

### 3.3 | Particle escaping pathways around RBC

Given the vortex-like structures between two clustering RBCs, one may expect that these vortices should be able to capture small particles and trap them between the cells similar to earlier observations for microparticles.<sup>26</sup> In Figure 5, we illustrate such events, that is, the pathways by which particles can enter into the vortices from the main flow. For this, a line of tracer particles has been seeded into the central region between the two RBCs and their trajectories

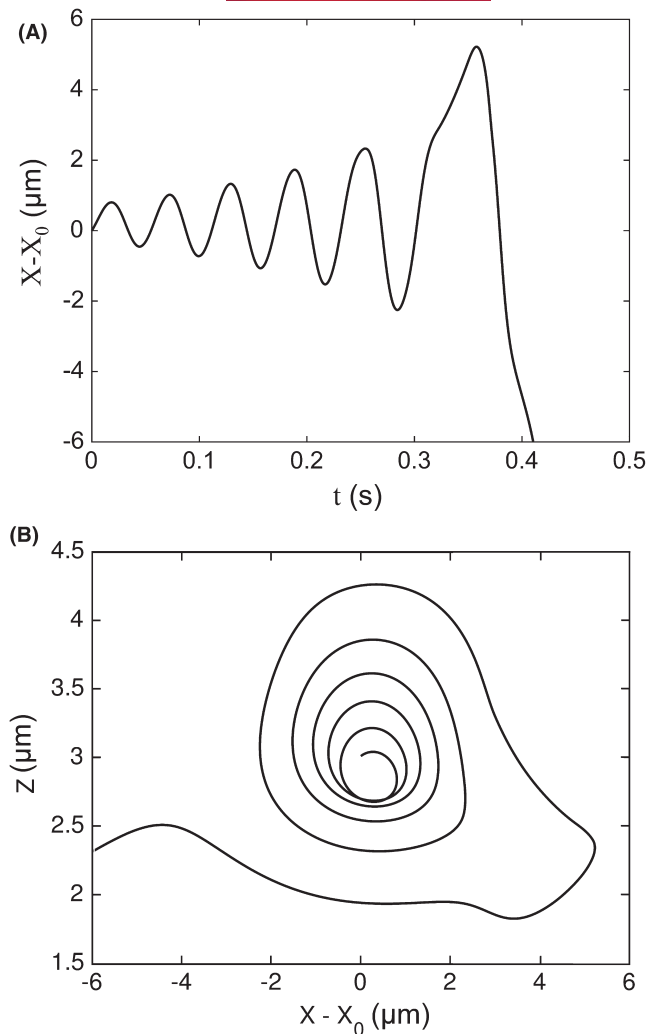


**FIGURE 6** Numerically calculated trajectories of a tracer escaping from flow vortices between two RBCs with velocity  $2.2 \text{ mm s}^{-1}$  where  $X_0$  is the center between the two RBCs. A, Temporal forward-backward motion along the direction of the flow. B, Toroidal trajectory in the x-y plane, starting from the middle and going outwards

integrated backward in time. Thus, the colored lines illustrate the entry of tracer particles into the vortices.

As can be seen in the streamlines in Figure 3, the vortices between two flowing RBCs typically are not fully closed. One can therefore expect that tracer particles should, depending on their initial position, also be able to escape from these vortices back into the main flow. Indeed, we do observe such trajectories as illustrated in Figure 6. Note that, in the experiment the period  $T$  is not affected by the projective view. For a fixed distance between the cells  $d_{\text{RBC}}$ , we find that the period  $T$  remains constant, independent of the amplitude in x-direction. This result is supported by numerical simulations (see Figure 6). Here, a particle first performs a spiraling motion between the two RBCs but eventually escapes from the region between the two RBCs. Due to the short observation time, we were unfortunately not able to observe such trajectories in the experiment (Figure 1 in Supplementary Material).

## 4 | DISCUSSION

Using PTV experiments, we measured the flow field around RBCs flowing in small microchannels. For isolated RBCs, we found a significant difference in the flow field depending on whether the RBC is in the croissant or in the slipper state. At the rear of a slipper, a small but characteristic vortex-like structure was observed. If two cells flow in close vicinity to each other in the croissant shape, another toroidal vortex-like structure appears between the cells as predicted by earlier numerical simulations.<sup>19,20,22,26</sup> However, while in earlier work numerical simulations of flowing RBCs have been compared with experiments only with respect to the shape of the RBCs, we here also compare the surrounding flow field.

Our rectangular channels could reproduce trapping events, as was also observed in simulations involving cylindrical channels.<sup>26</sup> Thus, it is very likely that such trapping could occur in vivo for a very dilute suspension of cells. Of course, cylindrical channels reflect better the in vivo situation, but our experiments needed a good optical access to the flowing tracer particles which was only granted by a flat optical window, that is, the by coverslip that was used to seal our channels. We showed that the rotation period in these vortices follows a quasi-linear law as a function of the distance between the red blood cells. Our experimental results show good similarities with numerical boundary-integral simulations. Nevertheless, a non-negligible discrepancy between the simulations and experimental results can be observed. This can be attributed to the fact that RBCs were not at a steady state in our simulations nor in experiments and disturbances in the flow field could occur. Our simulations could however illustrate qualitatively the trapping and escape of tracer particles from the vortex structures between the cells, which in principle could contribute to the transport and mixing properties of potential nanoparticle drug delivery agents. However, even in our artificial in vitro setup the flow seems not to be sufficiently stable that we could reproduce these events experimentally; thus, trapping of particles due to the flow field of single or diluted RBCs might rarely be the case in vivo.

## 5 | PERSPECTIVES

We provide experimental evidence of the presence of vortices around different shapes of red blood cells in capillary flow, and we characterize their velocity. The experimental findings are confirmed and extended by numerical simulations. This provides the basis for a quantitative description of capillary blood flow and drug delivery by micro- or nanoparticles.

## ACKNOWLEDGMENTS

F.Y., T.J., and C.W. acknowledge funding from the French German University (DFH /UFA). C.W. acknowledges funding from the DFG FOR 2688—Wa1336/12. F. Y. and T. P. acknowledge support from CNES and LabEx Tec21. S.G. acknowledges funding from the DFG

FOR 2688—GE2214/2-1. We gratefully acknowledge computing time provided by the SuperMUC system of the Leibniz Rechenzentrum, Garching, and by the Bavarian Polymer Institute. Open Access funding enabled and organized by Projekt DEAL.

#### DATA AVAILABILITY STATEMENT

Data are available from the authors upon reasonable request.

#### ORCID

Stephan Gekle  <https://orcid.org/0000-0001-5597-1160>

Thomas Podgorski  <https://orcid.org/0000-0001-6469-9170>

Christian Wagner  <https://orcid.org/0000-0001-7788-4594>

#### REFERENCES

- Vlahovska PM, Barthès-Biesel D, Misbah C. Flow dynamics of red blood cells and their biomimetic counterparts. *C R Phys*. 2013;14:451-458.
- Freund JB. Numerical simulation of flowing blood cells. *Annu Rev Fluid Mech*. 2014;46:67-95.
- Secomb TW. Blood flow in the microcirculation. *Annu Rev Fluid Mech*. 2017;49:443-461.
- Guest MM, Derrick JR, Cooper RG, Bond TP. Red blood cells change in shape in capillaries. *Science*. 1963;142:1319-1321.
- Gaehtgens P, Dührssen C, Albrecht KH. Motion, deformation and interaction of blood cells and plasma during flow through narrow capillary tubes. *Blood Cells*. 1980;6:799.
- Tomaiuolo G, Simeone M, Martinelli V, Rotoli B, Guido S. Red blood cell deformation in microconfined flow. *Soft Matter*. 2009;5:3736.
- Quint S, Christ AF, Guckenberger A, et al. 3D Tomography of cells in micro-channels. *Appl Phys Lett*. 2017;111:103701.
- Kihm A, Kaestner L, Wagner C, Quint S. Classification of red blood cell shapes in flow using outlier tolerant machine learning. *PLoS Comput Biol*. 2018;14:e1006278.
- Guckenberger A, Kihm A, John T, Wagner C. Numerical-experimental observation of shape bistability of red blood cells flowing in a microchannel. *Soft Matter*. 2018;14:2032-2043.
- Noguchi H, Gompper G. Shape transition of fluid vesicles and red blood cells in capillary flows. *Proc Natl Acad Sci USA*. 2005;102:14159-14164.
- Shi L, Pan TW, Glowinski R. Deformation of single red blood cell in bounded Poiseuille flows. *Phys Rev E*. 2012;85:016307
- Tahiri N, Biben T, Ez-Zahraouy H, Benyoussef A, Misbah C. On the problem of slipper shapes of red blood cells in the microvasculature. *Microvasc Res*. 2013;85:40.
- Lazaro GR, Hernandez-Machado A, Pagonabarraga I. Rheology of red blood cells under flow in highly confined microchannels: I. Effect of elasticity. *Soft Matter*. 2014;10:7195.
- Fedosov DA, Peltomäki M, Gompper G. Deformation and dynamics of red blood cells in flow through cylindrical microchannels. *Soft Matter*. 2014;10:4258.
- Lanotte L, Mauer J, Mendez S, et al. Red cells dynamic morphologies govern blood shear thinning under microcirculatory flow conditions. *Proc Nat Acad Sci USA*. 2016;113:13289.
- Ye T, Shi H, Peng L, Li Y. Numerical studies of a red blood cell in rectangular microchannels. *J Appl Phys*. 2017;122:084701.
- Reichel F, Mauer J, Nawaz AA, Gompper G, Guck J, Fedosov DA. High-throughput microfluidic characterization of erythrocyte shapes and mechanical variability. *Biophys J*. 2019;114:117.
- Takeishi N, Rosti ME, Imai Y, Wada S, Brandt L. Haemorheology in dilute, semi-dilute and dense suspensions of red blood cells. *J Fluid Mech*. 2019;872:818.
- McWhirter JL, Noguchi H, Gompper G. Deformation and clustering of red blood cells in microcapillary flows. *Soft Matter*. 2011;7:10967.
- McWhirter JL, Noguchi H, Gompper G. Flow-induced clustering and alignment of vesicles and red blood cells in microcapillaries. *Proc Natl Acad Sci USA*. 2009;106:6039.
- Tomaiuolo G, Lanotte L, Ghigliotti G, Misbah C, Guido S. Red blood cell clustering in Poiseuille microcapillary flow. *Phys Fluids*. 2012;24:051903.
- Ghigliotti G, Selmi H, Asmi LE, Misbah C. Why and how does collective red blood cells motion occur in the blood microcirculation? *Phys Fluids*. 2012;24:101901.
- Brust M, Aouane O, Thiébaud M, et al. The plasma protein fibrinogen stabilizes clusters of red blood cells in microcapillary flows. *Sci Rep*. 2014;4:4348.
- Claveria V, Aouane O, Thiébaud M, et al. Clusters of red blood cells in microcapillary flow: hydrodynamic versus macromolecule induced interaction. *Soft Matter*. 2016;12:8235.
- Aouane O, Farutin A, Thiébaud M, Benyoussef A, Wagner C, Misbah C. Hydrodynamic pairing of soft particles in a confined flow. *Phys Rev Fluids*. 2017;2:063102.
- Takeishi N, Imai Y. Capture of microparticles by bolus flow of red blood cells in capillaries. *Sci Rep*. 2017;7:5381.
- Lew H, Fung Y. The motion of the plasma between the red cells in the bolus flow. *Biorheology*. 1969;6:109.
- Nanne EE, Aucoin CP, Leonard EF. Molecular movement of bovine albumine in flowing suspensions of bovine erythrocytes. *Chem Eng Sci*. 2010;65:6389.
- Toy R, Hayden E, Shoup C, Baskaran H, Karathanasis E. The effects of particle size, density and shape on margination of nanoparticles in microcirculation. *Nanotechnology*. 2011;22:115101.
- Lee TR, Choi M, Kopacz AM, Yun SH, Liu WK, Decuzzi P. On the near-wall accumulation of injectable particles in the microcirculation: smaller is not better. *Sci Rep*. 2013;3:2079.
- Zhang H, Misbah C. Lattice Boltzmann simulation of advection-diffusion of chemicals and applications to blood flow. *Comput Fluids*. 2019;187:1.
- Liu Z, Clausen JR, Rao RR, Aidun CK. A unified analysis of nano-to-microscale particle dispersion in tubular blood flow. *Phys Fluids*. 2019;31:081903.
- Liu Z, Clausen JR, Rao RR, Aidun CK. Nanoparticle diffusion in sheared cellular blood flow. *J Fluid Mech*. 2019;871:636.
- Prothero J, Burton A. The physics of blood flow in capillaries: I. the nature of the motion. *Biophys J*. 1961;1:565.
- Aroesty J, Gross JF. Convection and diffusion in the microcirculation. *Microvasc Res*. 1970;2(3):247.
- Gekle S. Dispersion of solute released from a sphere flowing in a microchannel. *J Fluid Mech*. 2017;819:104.
- Amini H, Lee W, Di Carlo D. Inertial microfluidic physics. *Lab Chip*. 2014;14:2739.
- Zurita-Gotor M, Blawzdziwicz J, Wajnryb E. Swapping trajectories: a new wall-induced cross-streamline particle migration mechanism in a dilute suspension of spheres. *J Fluid Mech*. 2007;592:447.
- Lee W, Amini H, Stone HA, Di Carlo D. Dynamic self-assembly and control of microfluidic particle crystals. *PNAS*. 2010;28:22413.
- Ohmura T, Ichikawa M, Kamei K, Maeda YT. Oscillation and collective conveyance of water-in-oil droplets by microfluidic bolus flow. *Appl Phys Lett*. 2015;107:074102.
- Shin Y, Han S, Jeon JS, et al. Microfluidic assay for simultaneous culture of multiple cell types on surfaces or within hydrogels. *Nat Protoc*. 2012;7:1247.
- Kim S, Karrila S. *Microhydrodynamics*. Dover; 2005.
- Pozrikidis C. *Boundary integral and singularity methods for linearized flow*. Cambridge: Cambridge University Press; 1992.
- Guckenberger A, Schraml M, Chen PG, Leonetti M, Gekle S. On the bending algorithm for soft objects in flows. *Comput Phys Commun*. 2016;207:1.

45. Guckenberger A, Gekle S. Theory and algorithms to compute Helfrich bending forces: a review. *J Phys Cond Mat*. 2017;29:203001.
46. Bruus H. *Theoretical microfluidics*. Oxford: Oxford University Press; 2007.
47. Kuhlmann H, Romano F. The Lid-Driven Cavity. In: A. Gelfgat (Ed.), *Computational Modelling of Bifurcations and Instabilities in Fluid Dynamics*. New York: Springer; 2018.

**How to cite this article:** Yaya F, Römer J, Guckenberger A, et al. Vortical flow structures induced by red blood cells in capillaries. *Microcirculation*. 2021;28:e12693. <https://doi.org/10.1111/micc.12693>

#### SUPPORTING INFORMATION

Additional supporting information may be found online in the Supporting Information section.